Testing density functionals for structural phase transitions of solids under pressure: Si, SiO_2, and Zr

Bing Xiao,[1,*] Jianwei Sun,[1] Adrienn Ruzsinszky,[1] Jing Feng,[2] Robin Haunschild,[3] Gustavo E. Scuseria,[3,4,5] and John P. Perdew[1]

[1]*Department of Physics, Temple University, Philadelphia, Pennsylvania 19122, USA*

[2]*School of Engineering and Applied Science, Harvard University, Cambridge, Massachusetts 02138, USA*

[3]*Department of Chemistry, Rice University, Houston, Texas 77005, USA*

[4]*Department of Physics and Astronomy, Rice University, Houston, Texas 77005, USA*

[5]*Chemistry Department, Faculty of Science, King Abdulaziz University, Jeddah 21589, Saudi Arabia*

(Received 20 August 2013; published 12 November 2013)

We have investigated the structural phase transitions of crystalline Si (insulator-metal), SiO_2 (insulator-insulator), and Zr (metal-metal) under pressure, as a test of several density functionals for the exchange-correlation energy. While meta-generalized gradient approximations (meta-GGAs) such as revTPSS (revised Tao-Perdew-Staroverov-Scuseria) are more sophisticated than GGAs such as PBE (Perdew-Burke-Ernzerhof), and are more accurate without empiricism for atomization energies of molecules, lattice constants of solids, and surface energies, we confirm that these meta-GGAs tend to give smaller and less realistic transition pressures than the PBE GGA does. But we also show that the recent functionals of the meta-GGA made simple family (MGGA_MS) behave differently, predicting larger and often more realistic transition pressures. We suggest that further refinement of the meta-GGA can lead to a functional that is more accurate for properties of molecules and solids at equilibrium or under compression. We also show that, contrary to recent suggestions but in line with older ones, an accurate fundamental gap in the noninteracting band structure is not necessary for an accurate prediction of the transition pressure. Unlike the semilocal GGAs and meta-GGAs, and unlike the local density approximation also tested here, the screened hybrid functional HSE06 (Heyd-Scuseria-Ernzerhof) is fully nonlocal and predicts more realistic fundamental gaps. HSE06 is better than the semilocal functionals for the transition pressures of Si and SiO_2, but seriously overestimates the transition pressure in Zr. Besides the transition pressures, we report the transition energies and volumes, binding energy curves, and structural parameters at zero and transition pressure. Finally, we discuss how the performance of a functional can reflect its plottable exchange enhancement factor, and why the structural phase transitions are especially challenging for approximate density functionals.

DOI: 10.1103/PhysRevB.88.184103 PACS number(s): 71.15.Mb, 64.70.K−, 81.30.−t

I. INTRODUCTION: OLD AND NEW FUNCTIONALS AND THEIR PERFORMANCE

A. Density functional theory

In density functional theory (DFT),[1–5] the approximate exchange-correlation energy functionals are often sorted onto the five rungs of Jacob's ladder.[6,7] The lowest rung is the local spin-density approximation (LSDA), in which the exchange-correlation energy density is constructed from the local spin densities alone:[1–3]

$$E_{\rm xc}^{\rm LSDA}[n_\uparrow,n_\downarrow] = \int n(\vec{r})\varepsilon_{\rm xc}^{\rm unif}(n_\uparrow(\vec{r}),n_\downarrow(\vec{r}))d^3r, \quad (1)$$

where $n(\vec{r}) = n_\uparrow(\vec{r}) + n_\downarrow(\vec{r})$ is the total electron density and $\varepsilon_{\rm xc}^{\rm unif}(n_\uparrow,n_\downarrow)$ is the exchange-correlation energy per particle of a uniform electron gas. Note that in the spin-unpolarized case we have the local density approximation (LDA). Since LSDA starts from the spin-resolved uniform electron density, it is more accurate for compact crystal structures with slowly varying densities than it is for atoms and loosely bonded crystals where the electron density distribution is less uniform. As a result, LSDA overestimates the atomization energy for molecules and solids. The exchange-correlation hole of local spin density is not localized enough for atoms, placing their energies too high relative to those of molecules and solids.[8] For the same reason, the LSDA adsorption energy is too big, but the LSDA surface energy of a metal is fairly good.

All GGA-level functionals stand on the second rung of Jacob's ladder.[6,7] The GGA exchange-correlation energy is

$$E_{\rm xc}^{\rm GGA}[n_\uparrow,n_\downarrow] = \int n\varepsilon_{\rm xc}^{\rm GGA}(n_\uparrow,n_\downarrow,\nabla n_\uparrow,\nabla n_\downarrow)d^3r. \quad (2)$$

In this equation, $\nabla n_\uparrow$ and $\nabla n_\downarrow$ are the local spin-density gradients. The improvement of GGA over LSDA is significant, as reported in the literature.[9] GGA-level functionals correct the overbinding problem of LSDA: The GGA atomization energy is closer to experiment than that of LSDA, because the GGA correction to LSDA lowers the energy more for atoms than for molecules or solids. However, the GGA lattice constants are usually overestimated for solids, and thus the mechanical moduli are underestimated. Moreover, GGA functionals are unable to predict the correct absorption energy and surface energy simultaneously; they usually overestimate the adsorption energy but underestimate the surface energy. Some GGA functionals such as revPBE[10] and RPBE[11] are specifically modified from PBE[9] for adsorption problems. Other GGA functionals such as AM05,[12,13] Wu and Cohen (WC),[14] PBEsol,[15] and SOGGA[16] are especially designed for solid structural calculations. The exchange part of a "GGA for solids" has a weakened dependence on the reduced density gradient

$$s = |\nabla n| / [2(3\pi^2)^{1/3} n^{4/3}] \quad (3)$$

in comparison with PBE, revPBE, etc.

AM05, WC, PBEsol, and SOGGA significantly improve the accuracy of lattice constants and bulk moduli, but they are less

accurate than PBE for energetics (energy barrier and cohesive energy). These results illustrate the well-known dilemma that for GGAs the geometry and energetics cannot be much improved at the same time. Good geometry requires recovering the gradient expansion for exchange at small s, while good energetics requires an exchange gradient coefficient almost twice as big.[15,17,18]

B. Meta-generalized gradient approximations

The third rung of Jacob's ladder is the meta-GGA. Besides the electron density and its gradient, one more ingredient is included in the construction, namely, the orbital kinetic energy density $\tau_\sigma(r) = \frac{1}{2}\sum_i |\nabla\phi_i^\sigma(r)|^2$, where $\phi_i^\sigma(r)$ is the occupied Kohn-Sham spin orbital from a self-consistent one-particle Schrödinger equation. Now one may write the exchange-correlation energy of the system as

$$E_{\rm xc}^{\text{meta-GGA}}[n_\uparrow,n_\downarrow] = \int n\varepsilon_{\rm xc}^{\text{meta-GGA}}(n_\uparrow,n_\downarrow,\nabla n_\uparrow,\nabla n_\downarrow,\tau_\downarrow,\tau_\uparrow)d^3r. \quad (4)$$

Meta-GGA is almost as computationally efficient as GGA, because both require only a single integration over three-dimensional space.

Some meta-GGAs employ the Laplacian of the electron density along with or in place of the kinetic energy density. Many different forms are available, including Perdew,[19] Ghosh and Parr,[20] Becke and Roussel,[21] Van Voorhis and Scuseria,[22] Schmider and Becke,[23] Perdew, Kurth, Zupan, and Blaha,[24] Tao, Perdew, Staroverov, and Scuseria (TPSS),[25] revised Tao, Perdew, Staroverov and Scuseria (revTPSS),[26] Zhao and Truhlar (M06-L),[27] the regularized revTPSS (regTPSS),[28] and the meta-GGA made simple (MGGA_MS) family of density functionals.[29,30] In this paper, we will test only a few meta-GGA functionals, those designed for solids and surfaces as well as for molecules (TPSS, revTPSS, regTPSS, and MGGA_MS). The exchange energy of these meta-GGAs can be written as

$$E_x^{\text{meta-GGA}}[n] = \int n\varepsilon_x^{\rm unif}(n)F_x(s,\alpha)d^3r \quad (5)$$

for a spin-unpolarized electron density n ($n_\uparrow = n_\downarrow = n/2$). Here $\varepsilon_x^{\rm unif}(n) = -\frac{3}{4\pi}(3\pi^2 n)^{1/3}$ is the exchange energy per electron of the uniform electron gas. GGA exchange can be written similarly, but without the α dependence. α is another dimensionless quantity defined by

$$\alpha = (\tau - \tau^W)/\tau^{\rm unif} = (5s^2/3)(z^{-1} - 1), \quad (6)$$

where $z = \tau^W/\tau$. Here $\tau = \sum_\sigma \tau_\sigma$ is the orbital kinetic energy density, $\tau^W = |\nabla n|^2/8n$ is its von Weizsäcker approximation (exact for one- and two-electron densities), and $\tau_{\rm unif} = \frac{3}{10}(3\pi^2)^{2/3}n^{5/3}$ is its Thomas-Fermi approximation (exact for uniform densities). For the general spin-polarized case, the total exchange energy is calculated from the spin-scaling relationship.[31]

$$E_x[n_\uparrow,n_\downarrow] = \tfrac{1}{2}(E_x[2n_\uparrow] + E_x[2n_\downarrow]). \quad (7)$$

α is employed to recognize and give different GGA treatments to different kinds of density regions. In one- and two-electron regions (including covalent-single bonds), $\alpha = 0$. For a region of slowly varying density (as in a metal), $\alpha = 1$. Additionally, in the region where two closed shells overlap, $\alpha \gg 1$.

TPSS[25] was constructed nonempirically to satisfy many exact constraints on the exchange-correlation energy. revTPSS[26] revised the TPSS form to incorporate insights from the PBEsol GGA for solids. Both of these meta-GGAs, however, have a spurious order-of-limits problem: The exchange enhancement factor $F_x(s=0,\alpha=0)$ depends upon whether s or α tends to zero first. regTPSS[28] regularized the revTPSS form by removing this problem.

The s and α dependencies of F_x are tangled in most meta-GGAs. MGGA_MS is the first meta-GGA functional that separates them.[29] The enhancement factor is taken to be

$$F_x^{\text{MGGA\_MS}}(s,\alpha) = F_x^1(s) + f(\alpha)\big[F_x^0(s) - F_x^1(s)\big]. \quad (8)$$

The function $f(\alpha)$ interpolates between $\alpha = 0$ and 1, then extrapolates to $\alpha \gg 1$. The latter situation arises when two closed-shell atoms overlap, and in fact MGGA_MS gives a much more reliable description of the intermediate range of the van der Waals interaction than do TPSS, revTPSS, and regTPSS. We have argued[32] that the meta-GGA ingredient α can recognize covalent, metallic, and weak bonds. In MGGA_MS, the order-of-limits problem is naturally avoided.

Two other variants of the MGGA_MS functional have also been constructed recently.[30] For convenience, we refer to all three variants as the meta-GGA made simple family of density functionals. While the original MGGA_MS0 was not fitted to data sets, the MGGA_MS1 has one fit parameter and the MGGA_MS2 has two. The additional freedom allows tuning the exchange enhancement factor in the large-α region. Fits were made to the molecular test sets G2/97 (Refs. 33 and 34) and BH42,[35] including atomization energies and barrier heights to chemical reactions. Some preliminary tests[29,30,32] on the MGGA_MS family of density functionals suggest that they are more accurate for a variety of ground state properties of molecules and solids than previous semilocal meta-GGA, GGA, and LSDA functionals, especially where van der Waals (vdW) interaction is important.

The meta-GGA functionals TPSS, revTPSS, and MGGA_MS have been tested for the equilibrium geometries and energetics of molecules and solid structures, and their performances compared with those of GGA and LSDA functionals.[29,30,32,36–38] These previous calculations showed that meta-GGA can predict good lattice constants, surface energies, and cohesive energies at the same time. The meta-GGA seems to be able to step out of the geometry-energy dilemma encountered in GGA functionals.[39,40]

C. Phase transitions of solids under pressure

Phase transitions are important in solid-state physics and materials science, and also relevant to the geometry-energy dilemma. Indeed, it was early work by Hamann[41] on the SiO_2 phase transition under pressure that motivated many solid-state physicists to switch from LSDA to the PBE GGA. Can a meta-GGA predict good results for the equilibrium lattice properties of two polymorphs of a solid, as well as the phase transition parameters such as energy difference and transition pressure, simultaneously? To address this question, we considered three different types of phase transition induced by pressure. The

first example is the diamond-structure Si (D-Si) to β-tin Si transition, an insulator-to-metal transformation. The second one is a normal insulator-to-insulator phase transition in SiO_2, the α-quartz to stishovite transition. The phase transition parameters and equilibrium lattice properties of the first two examples have been calculated via the random phase approximation (RPA) in our previous work.[42] In the third example, we have considered the metal-to-metal structural transition from ω-Zr to β-Zr. Our calculations will show that these transitions are very sensitive tests of approximate density functionals, and that earlier meta-GGAs can fail badly for the transition pressure. This failure was first pointed out by Wilkins and collaborators.[43,44] We confirm and extend their results here, but we also find that the MGGA_MS functionals are promising for phase transitions.

II. METHODS AND DETAILS

A. Density functional calculations

All first-principles calculations with periodic boundary conditions employed the VASP program (Vienna *ab initio* simulation program), which uses the projector augmented wave (PAW) method.[45] In the PAW method, the frozen-core approximation is used, and the pseudoatom is described by PAW pseudopotentials. For the plane-wave expansions, the kinetic energy cutoff was set to 500 eV for all calculations. The GW-type PAW potentials for Si, O, and Zr were employed in this work: Si_{3s3p3d}, O_{2s2p}, and $Zr_{4s4p4d5s}$. These special PAW potentials were constructed by Kresse and co-workers in their RPA calculations,[46] with accurate scattering properties up to $\sim$10 Ry above the vacuum level. The core radii for Si, O, and Zr pseudoatoms were 0.840, 0.672, and 1.06 Å, respectively. The energy integrations were performed in the first irreducible Brillouin zone, and the methods used for generating the k mesh depended on the space group of the crystal structures. For cubic (D-Si and β-Zr) and tetragonal (β-tin Si and stishovite) phases, we used the Monkhorst-Pack method to generate $16 \times 16 \times 16$ and $12 \times 12 \times 14$ k meshes for optimizing the crystal structures, respectively.[47] The k grids used for α-quartz (trigonal) and ω-Zr (hexagonal) were $14 \times 14 \times 10$ and $15 \times 15 \times 19$, respectively, and were generated by the Γ-centered method. Similar k grids were also used to calculate the energy-volume curve for each phase. Using the present settings, the total energy was converged to 1 meV.

The exchange-correlation energy was approximated using functionals on the first three rungs of Jacob's ladder, including the Perdew-Zunger LDA,[48] the PBE GGA,[9] PBE modified for solids (PBEsol),[15] the Tao-Perdew-Staroverov-Scuseria meta-GGA (TPSS),[25] the revised TPSS (revTPSS),[26] the regularized revTPSS (regTPSS),[28] and the meta-GGA made simple (MGGA_MS0)[29] and its other two variants (MGGA_MS1 and MGGA_MS2).[30] The self-consistent implementation of regTPSS and the MGGA_MS family of density functionals in the VASP code can be found in our recent works.[28–30]

For some structures, the transition pressures were also estimated from other exchange-correlation functionals, including the Heyd-Scuseria-Ernzerhof screened hybrid functional (HSE06, which mixes the nonlocal Hartree-Fock-type exchange in the short-range portion of the electron-electron interaction with PBE exchange),[49–52] and various GGAs: Perdew-Wang 91 (PW91, a parent of PBE),[53] Armiento-Mattsson (AM05, an early GGA for solids),[12,13] WC,[14] and RPBE.[11]

For the screened hybrid functional HSE06, we employed different k meshes for all six phases, i.e., D-Si ($10 \times 10 \times 10$), β-tin Si ($8 \times 8 \times 10$), α-quartz SiO_2 ($8 \times 8 \times 6$), stishovite ($8 \times 8 \times 10$), ω-Zr ($8 \times 8 \times 10$), and β-Zr ($10 \times 10 \times 10$). Employing the *downsampling* method reduces the computing time significantly. The total energy was converged to 5 meV/atom. In the VASP code, the default range separation parameter μ is 0.20 $Å^{-1}$ for the semilocal and nonlocal parts of the exchange functional. The same value was used in our current work.

The calculations using the PW91 and WC functionals were carried out in the CASTEP code.[54] The crystal structures were reoptimized by ultrasoft pseudopotentials (USPPs) for Si, O, and Zr atoms. The plane-wave cutoff was set to 500 eV, and k grids similar to those presented previously were employed.

B. Phonon calculations

The zero-point energy and finite-temperature correction to the transition pressure can be obtained from the phonon spectrum. In this work, we have calculated the phonon spectra of SiO_2 structures using density functional perturbation theory in the CASTEP code.[54] For Si and Zr systems, the phonon effects on the transition pressures were taken from the literature. In our phonon calculations, the plane-wave basis set was expanded in reciprocal space with a kinetic energy cutoff of 550 eV. USPPs were used to represent the pseudoatoms of Si and O, i.e., Si ($3s^2 3p^2$) and O ($2s^2 2p^4$). For the energy integrations in the first irreducible Brillouin zone, the Monkhorst-Pack method was used to generate $6 \times 6 \times 8$ and $4 \times 4 \times 4$ k meshes for stishovite and α-quartz, respectively. The convergence tests with respect to k points were carefully conducted. For the exchange-correlation energy, only the PBE GGA was employed, because previous studies showed that different density functionals usually give quite similar results for the zero-point energy (ZPE) and thermal correction to the phase transition pressure.[55] The obtained ZPE and finite-temperature correction at each cell volume were added to the energy-volume curves. The change of the transition pressure induced by these two factors can be calculated from the change of the common tangent line of the energy-volume curves for the two phases.

The predicted lattice constants tabulated in this paper do not include the small phonon effects. This makes them more comparable to results in the earlier literature.

C. Equation of state

In order to evaluate the transition pressure and other structural parameters (cell volume, bulk modulus, and its pressure derivative), the obtained energy-volume curves of the six phases were fitted to the analytic third-order Birch-Murnaghan[56,57] equation of state (EOS) for $E(V)$, the total energy of the unit cell of volume V, which may include the ZPE and finite-temperature correction. Parameters in this equation include E_0 (the equilibrium energy) and V_0 (the equilibrium cell volume), as well as B_0 and B_0' (the bulk modulus and its

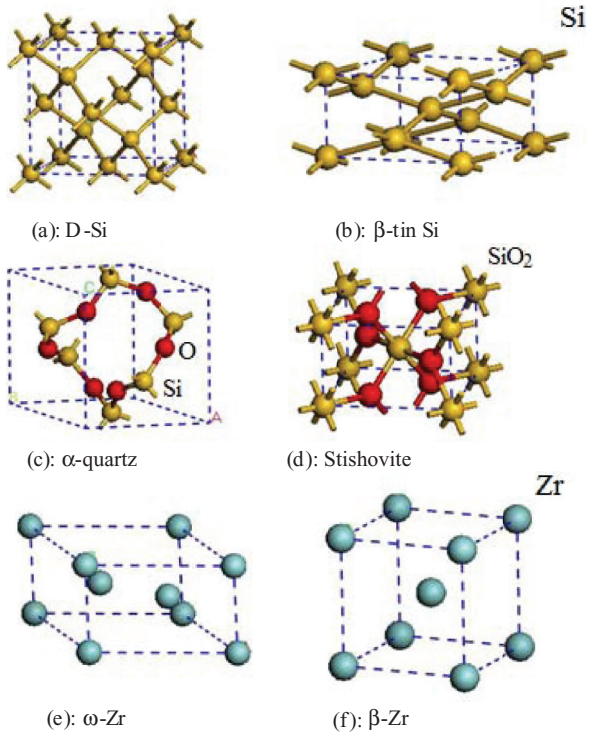

FIG. 1. (Color online) The crystal structures of Si, SiO_2, and Zr polymorphs: (a) D-Si (LP), (b) β-tin Si (HP), (c) α-quartz (LP), (d) stishovite (HP), (e) ω-Zr (LP), and (f) β-Zr (HP). Note that, for the SiO_2 structures, the red balls are oxygen atoms and the yellow ones are silicon atoms.

pressure derivative dB/dP). The pressure of a single phase at volume V is $-dE/dV$. The common tangent line to the high-pressure (HP) and low-pressure (LP) curves (per formula unit) can be calculated analytically from the Birch-Murnaghan expressions for the two phases. Minus the slope of this tangent line is the theoretical transition pressure, at which both phases can coexist for all possible volume fractions.

In this paper, we have also evaluated the transition volume (V_t) for each phase, which is given by the solution of

$$P(V_t) = \frac{3}{2}B_0\left[\left(\frac{V_0}{V_t}\right)^{7/3} - \left(\frac{V_0}{V_t}\right)^{5/3}\right] \times \left\{1 + \frac{3}{4}(B_0' - 4)\left[\left(\frac{V_0}{V_t}\right)^{2/3} - 1\right]\right\}. \quad (9)$$

Here $P(V_t)$ is the pressure, which we set to the *experimental* transition pressure before the corresponding transition volume V_t is computed[43] for comparison with experiment. The theoretical transition pressures are sometimes inaccurate, due mainly to errors in E_0 and not to errors in the other parameters of the equation of state. In other words, the largest error in the theoretical transition pressure arises because the EOS of one phase displays an erroneous rigid vertical shift with respect to that of the other.

D. Crystal structures

The crystal structures of Si, SiO_2, and Zr studied in this work are shown in Fig. 1. The most stable phase of Si has a crystal structure similar to diamond (diamond-Si or D-Si) with a fcc cell with space group $Fd\bar{3}m$ (227). There are eight atoms in the conventional cell. Experimentally, when the pressure is raised above 10 GPa, the D-Si phase transforms into the β-tin Si phase. The latter structure has four atoms in a body-centered-tetragonal conventional cell [space group $I4_1/amd$ (141)].[58,59]

The conventional cell of α-quartz has trigonal symmetry with space group $P3_221$(152), and each cell has three SiO_2

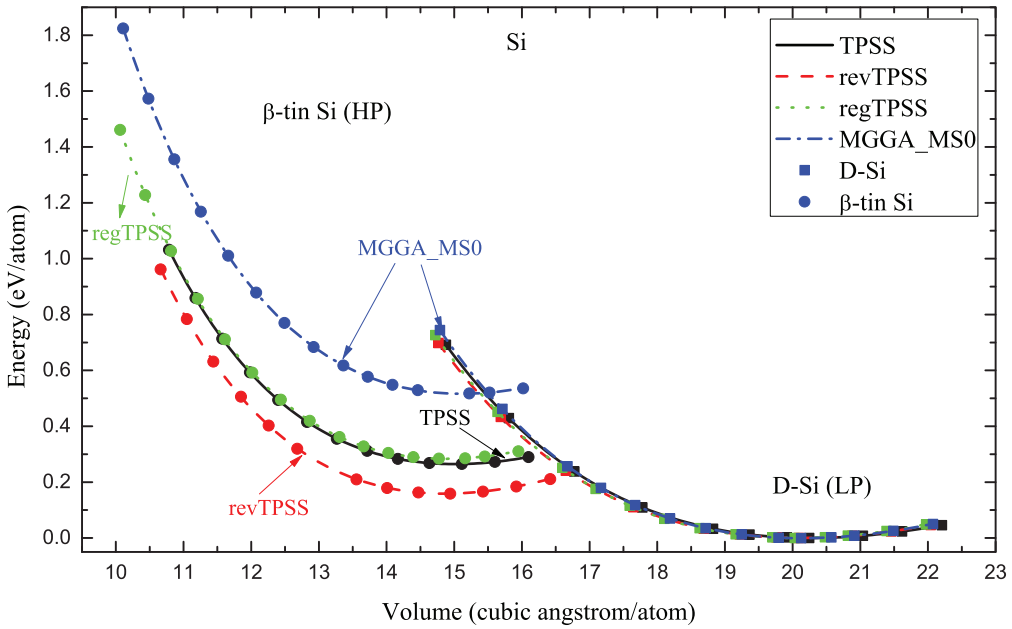

FIG. 2. (Color online) The total energies of D-Si (LP) and β-tin Si (HP) phases are calculated as a function of cell volume by four different MGGA exchange-correlation functionals. The total energies are given relative to the cell energy of the D-Si phase at the equilibrium volume for each MGGA functional. The dotted and solid lines are obtained from the third-order Birch-Murnaghan equation of state.

TABLE I. The structural and phase transition parameters of the D-Si (LP) and β-tin Si (HP) phases calculated by different exchange-correlation functionals. The zero-point energy and finite-temperature (300 K) correction to the transition pressure were estimated from the phonon spectra of the two phases using the PBE functional, and the value was found to be -1.3 GPa (Refs. 43 and 67). We define ΔE_0 and ΔV_0 as $\Delta E_0 = E_{\rm HP} - E_{\rm LP}$ and $\Delta V_0 = V_{\rm LP} - V_{\rm HP}$, where LP and HP refer to the high- and low-pressure phases, respectively. E and V are the total energy and volume at the equilibrium state. The a_t and ratio c_t/a_t are the values computed at the transition pressure (11.7 GPa) for the β-tin Si phase (Ref. 43). Because this transition is reversible under pressure, there is no experimental value for the equilibrium volume of the HP phase.

Properties	LDA	PBE	PBEsol	AM05	TPSS	revTPSS	regTPSS	MGGA_MS0	MGGA_MS1	MGGA_MS2	HSE06	Expt.
						D-Si						
a (Å)	5.4025	5.4650	5.4305	5.4315	5.4516	5.4380	5.4324	5.4408	5.4464	5.4270	5.4335	5.4288[a]
V_0 (Å^3/atom)	19.71	20.40	20.02	20.03	20.25	20.10	20.04	20.13	20.19	19.98	20.05	20.0[a]
	19.72[a]	20.48[a]	20.06[a]	20.07[a]							20.07[a]	
	17.61[b]	18.28[b]										
B (GPa)	97.1	89.4	94.4	93.6	92.4	94.1	99.0	101.8	99.9	102.1	101.5	99.2[a]
	96.4[a]	89.0[a]	93.9[a]	93.1[a]							99.1[a]	97.88[e]
	97[b]	91[b]										
B'	4.03	4.07	4.02	4.01	4.03	4.00	3.94	3.92	3.93	3.93	4.06	4.11[a]
	4.13[a]	4.12[a]	4.09[a]	4.08[a]							4.00[a]	4.24[e]
	4.0[b]	3.7[b]										
V_t (Å^3/atom)	17.87	18.38	18.10	18.10	18.28	18.17	18.19	18.29	18.34	18.18	17.90	18.15[a]
	17.86[a]	18.42[a]	18.13[a]	18.13[a]							18.21[a]	
						β-tin Si						
a (Å)	4.7613	4.8138	4.7801	4.7609	4.7787	4.7650	4.7520	4.6568	4.6758	4.6738	4.7602	
c_0/a_0	0.5489	0.5487	0.5487	0.5484	0.5504	0.5489	0.5615	0.5977	0.5921	0.5876	0.5491	
	0.548[a]	0.550[a]	0.548[a]	0.546[a]							0.565[a]	
	0.546[b]	0.547[b]										
V_0 (Å^3/atom)	14.81	15.30	14.98	14.80	15.02	14.85	15.06	15.09	15.13	15.00	14.81	
	14.82[a]	15.36[a]	15.02[a]	14.82[a]							15.10[a]	
	13.22[b]	13.69[b]										
B (GPa)	120.4	109.7	119.1	124.1	116.3	122.9	127.3	131.3	128.6	130.4	119.0	
	116.0[a]	106.4[a]	115.0[a]	120.5[a]							117.0[a]	
	117[b]	109[b]										
B'	4.1	4.3	4.13	4.08	4.24	4.15	4.01	3.95	4.01	3.99	4.32	
	4.59[a]	4.57[a]	4.52[a]	4.54[a]							4.35[a]	
	4.3[b]	4.1[b]										
V_t (Å^3/atom)	13.66	14.03	13.80	13.67	13.79	13.72	13.74	13.99	13.99	13.90	13.67	13.96[a]
	13.63[a]	14.04[a]	13.80[a]	13.67[a]							13.89[a]	
a_t (Å)	4.6456	4.6862	4.6707	4.6499	4.6581	4.6552	4.5992	4.6064	4.6159	4.6023	4.6611	4.6900[e]
c_t/a_t	0.5411	0.5449	0.5376	0.5434	0.5458	0.5397	0.5658	0.5681	0.5647	0.5673	0.5462	0.550[a,e]
	0.544[a]	0.544[a]	0.543[a]	0.543[a]							0.557[a]	

TABLE I. (*Continued.*)

Properties	LDA	PBE	PBEsol	AM05	TPSS	revTPSS	regTPSS	MGGA_MS0	MGGA_MS1	MGGA_MS2	HSE06	Expt.
Phase transition parameters												
ΔE_0 (eV/atom)	0.206	0.290	0.185	0.153	0.265	0.160	0.285	0.517	0.475	0.429	0.398	
	0.206[a]	0.287[a]	0.184[a]	0.152[a]	0.266[d]						0.390[a]	
	0.216[d]	0.299[d]									0.447[d]	
ΔV_0 (Å^3/atom)	4.90	5.10	5.04	5.24	5.24	5.25	4.98	5.04	5.06	4.98	5.35	
P_t (GPa)	5.7	8.4	4.8	3.5	7.3	3.7	8.0	17.3	15.4	13.9	13.3	10–14[a,c]
	5.8[a]	8.4[a]	4.8[a]	3.5[a]							12.4[a]	11–15[e]
	6.7[b]	9.2[b]										

[a]Reference 43.
[b]Reference 66.
[c]Reference 68.
[d]Reference 44.
[e]Reference 65.

units. Stishovite (density: 4.29 g/cm^3) has a more compact structure than α-quartz (2.65 g/cm^3), and is crystallized in a centered-tetragonal cell with space group $P4_2/mnm$ (136). In addition, there are two SiO_2 units in each conventional cell of stishovite. The α-quartz phase is stabilized over the stishovite phase below 7 GPa.[41,60] The transformation of α-quartz into stishovite also displays changes of coordination numbers of both Si and O atoms.

Finally, for the two polymorphs of Zr, the space groups are $Im\bar{3}m(229)$ and $P6/mmm$ (191) for β-Zr and ω-Zr, respectively.[61–63] The conventional cell of ω-Zr has three atoms and that of β-Zr has two. The ω-Zr to β-Zr transition occurs at 30 ± 2 GPa, and has been studied by energy-dispersive x-ray diffraction.[64] Ostanin *et al.*[61] reported that the transition pressure was 35 ± 5 GPa at 300 K in another experiment. These high transition pressures arise by combining unusually small structural energy and volume differences, and thus are especially challenging to approximate calculations.

III. RESULTS

A. D-Si-to-β-tin Si phase transition

Figure 2 shows the calculated energy-volume curves of D-Si and β-tin Si phases using the meta-GGA functionals TPSS, revTPSS, regTPSS, and MGGA_MS0. The results for other functionals are not given in the figure for simplicity. The figure shows that the functional errors are reflected mainly in erroneous vertical displacements of the curve for one phase with respect to that for the other.

In Table I, the optimized lattice properties and phase transition parameters of the D-Si and β-tin Si phases from different exchange-correlation functionals are compared with available experimental results. The equilibrium lattice constant of D-Si shows typical trends: too small in LDA, too large in PBE, about right in PBEsol, too large but improved over PBE in TPSS, and about right in the other meta-GGAs.

For the β-tin Si phase, the MGGA_MS family behaves differently from the other density functionals, giving a larger c/a ratio and thus apparently favoring cubic symmetry too much. The lattice constants of the β-tin Si phase measured at the transition pressure (11.3 GPa) are $a = 4.6900$ Å, and $c = 2.5780$ Å, with $c/a = 0.5496$.[65]

Experimentally, the bulk modulus of D-Si is 99.2 GPa.[43] Hu *et al.*[65] found 97.88 GPa using the measured elastic constants. Most functionals underestimate the bulk modulus of D-Si, but the screened hybrid functional HSE06 gives 101.49 and 99.1 GPa in this paper and in Ref. 43, respectively, with both values in good agreement with experiment. The MGGA_MS family of density functionals and regTPSS give the bulk modulus in better agreement with experiment than other semilocal functionals. For the β-tin Si phase in HSE06, we find a bulk modulus of 119.0 GPa, in good agreement with a previous reference.[43] Finally, for the calculated B', our results are slightly different from other references.[43,66] However, the agreement among reference values is also poor, indicating that B' is sensitive to the parametric fitting.

Hennig *et al.*[43] have calculated the energy difference between the two polymorphs using various methods, and their results are also shown in Table I. In their calculations,

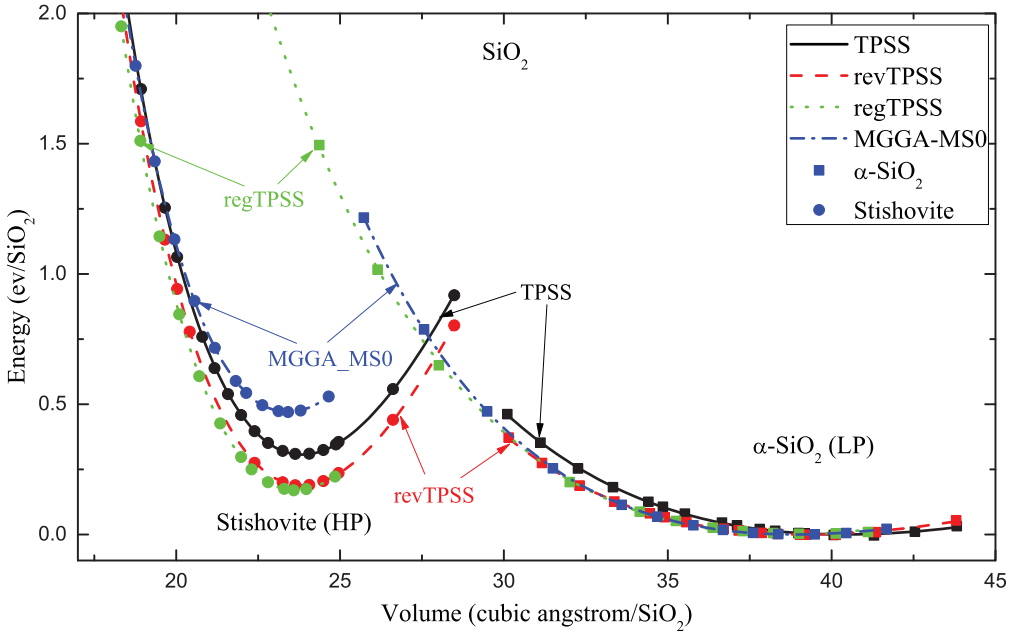

FIG. 3. (Color online) The calculated energy-volume curves of the α-quartz (LP) and stishovite (HP) phases. The total energies obtained by the meta-GGA functionals are given relative to the cell energy of the α-quartz phase at the equilibrium volume for each functional.

the quantum diffusion Monte Carlo method gives the most accurate values, which were found to be 0.480 eV/atom in Ref. 43 and 0.424 eV/atom in Ref. 44, respectively. LDA, the PBEsol GGA, and all of the meta-GGAs outside the MGGA_MS family seriously underestimate this energy difference, while the screened hybrid HSE06 performs well for it. Interestingly, regTPSS gives 0.285 eV/atom, which strongly improves the poor performance of revTPSS, suggesting that the order-of-limits error in revTPSS is significant here.

The errors of the various functionals for the transition energy are reflected in the transition pressure, which is seriously too low in LDA, PBEsol, and the meta-GGAs outside the MGGA_MS family. The phase transition pressure from D-Si to β-tin Si was found to be in the range of 10–15 GPa from quantum Monte Carlo (QMC).[43,55] Without including the ZPE and finite-T effect, the value obtained by HSE06 in this paper is 14.6 GPa. The finite-T and ZPE corrections further reduce the transition pressure from D-Si to β-tin Si by 1.3 GPa in Ref. 67 and 1.0 GPa in a recent calculation.[55] With these thermal corrections, HSE06 gives 13.3 GPa, which is larger than the 12.4 GPa reported in Ref. 42. The transition pressure predicted by RPA is also realistic, 12.2 GPa.[42] The transition volumes, calculated as described around Eq. (9), are reasonably good for all tested functionals.

B. α-quartz-to-stishovite SiO_2 phase transition

Figure 3 illustrates the energy-volume curves of the two SiO_2 phases using the meta-GGA functionals. We show the calculated structural and phase transition properties of the SiO_2 phases in Table II. As can be seen from Table II, the lattice constants of α-quartz are overestimated by most exchange-correlation functionals other than LDA, suggesting that a long-range vdW correction might be needed to shrink the lattice constants. In earlier work by Hamann,[41] the lattice constants of α-quartz were found to be $a = 4.84$ Å and $c = 5.41$ Å by LDA, but our calculation using LDA gives $a = 4.9041$ Å and $c = 5.3790$ Å. The large differences between the two results are probably associated with the different pseudopotentials used in Ref. 41 and in our paper. Below the meta-GGA level, PBEsol gives better lattice constants and equilibrium cell volume than other semilocal functionals. The lattice constants of α-quartz from the MGGA_MS functionals are only slightly worse than those of PBEsol and AM05. The MGGA_MS functionals are the only ones in Table II to include a reliable estimate of intermediate-range vdW effects;[30,32] none of these functionals includes the long-range effects.[69]

In Fig. 4, we show the equilibrium cell volumes of α-quartz obtained by different density functionals. The results of semilocal functionals are compared with the RPA.[42] RPA is able to capture the long-range vdW interactions in molecules and solids.[69] MGGA_MS0, MGGA_MS2, and HSE06 are better than other tested functionals for the equilibrium volume of α-quartz. In Sec. III D, we will employ pairwise corrections pioneered by Grimme[70] for the PBE and TPSS functionals to investigate the effect of long-range vdW interaction. The most accurate structural parameters of α-quartz are found from the screened hybrid HSE06. This is surprising, because HSE06 includes no long-range vdW interaction, although it is believed to give a good description of covalent bonds.[71]

The lattice constants of stishovite are rather accurate from all tested functionals. For the bulk modulus of α-quartz, Zupan *et al.*[66] found a PBE bulk modulus of 44 GPa, which is close to Hamann's value[41] but not to ours. For the bulk modulus of stishovite, both regTPSS and the MGGA_MS family of density functionals give results in agreement with experiment.[41,72,73] More recently, Driver and co-workers[74] have employed the QMC method, finding the bulk moduli of α-quartz and stishovite to be 32 and 305 GPa, respectively, with the former value somewhat different from experiment.

TABLE II. The structural and phase transition parameters of the α-quartz (LP) and stishovite (HP) phases of SiO_2 calculated by different exchange-correlation functionals. The ZPE and finite-temperature correction have been estimated from phonon calculations using PBE and are included in the calculated transition pressures (P_t); the correction was found to be $+0.577$ GPa. The definitions of ΔE_0 and ΔV_0 are the same as those given in Table I.

Properties	LDA	PBE	PBEsol	AM05	TPSS	revTPSS	regTPSS	MGGA_MS0	MGGA_MS1	MGGA_MS2	HSE06	Expt.
						α-Quartz						
a (Å)	4.9041	5.0153	4.9605	4.9613	5.0186	5.0044	5.0005	4.9740	4.9869	4.9736	4.9568	4.92,[a] 4.921[e]
	4.84[a]	4.97[a]										
c_0/a_0	1.0969	1.0951	1.0996	1.1004	1.0922	1.0945	1.0936	1.0933	1.0953	1.0933	1.0961	1.099,[a] 1.097[e]
	1.1177[a]	1.1107[a]										
	1.104[b]	1.099[b]										
V_0 (Å^3/SiO_2)	36.95	39.41	38.63	38.74	39.17	39.15	39.00	38.37	38.95	38.39	38.28	37.73[e]
B (GPa)	36.95	35.59	32.08	33.07	34.84	36.42	43.08	38.4	43.416	46.9	33.33	38,[a] 37.2[d]
	45[a], 35[b]	48[a], 44[b], 43[b]										36.5,[e] 37.4[e]
B'	5.48	4.68	6.05	4.58	3.92	4.07	3.88	4.97	4.19	3.86	5.44	6,[a] 6.0[d]
	4.9[a], 7.1[b]	3.0[a], 3.2[b], 3.3[b]										5.9,[e] 6.3[e]
V_t (Å^3/SiO_2)		34.62	33.48	34.05	34.51	33.71	33.82	33.87	34.30	33.69	33.90	
						Stishovite						
a (Å)	4.1516	4.225	4.1892	4.1935	4.1984	4.1972	4.1932	4.1901	4.1890	4.1717	4.1751	4.18[a]
	4.20,[a] 4.157[c]	4.29[a]										4.1777[c]
c_0/a_0	0.6417	0.6374	0.6394	0.6377	0.6400	0.6403	0.6399	0.6365	0.6380	0.6402	0.6382	0.6387[a]
	0.6309[a]	0.6247[a]										0.6381[c]
	0.642[b]	0.636[b]										
	0.6394[c]											
V_0 (Å^3/SiO_2)	22.96	24.04	23.51	23.52	23.68	23.68	23.59	23.42	23.45	23.24	23.22	23.30[c]
	22.96[c]											
B (GPa)	321.57	270.36	277.85	295.79	296.5	296.13	308.72	318.72	306.41	305.40	327.30	313[a]
	286,[a] 303,[b]	260,[a] 257,[b]										306 $\pm$ 4[c]
	313[c]	249[b]										295[d]
B'	4.21	4.42	4.52	4.32	4.22	4.23	4.14	4.12	4.35	6.09	4.11	2.8 $\sim$ 6[a]
	4.6,[a] 4.8[b]	3.0,[a] 4.9,[b]										3.2 $\pm$ 3.3[c]
	4.24[c]	5.0[b]										1.3[d]
V_t (Å^3/SiO_2)		23.54	23.08	23.02	23.28	23.27	23.10	22.88	23.01	22.78	22.72	
						Phase transition parameters						
ΔE_0 (eV/SiO_2)	-0.031	0.532	0.171	0.292	0.384	0.189	0.167	0.467	0.503	0.286	0.484	0.51–0.54[a]
	-0.090,[b] 0.02[a]	0.57,[a] 0.445[b]										0.525,[f] 0.48[f]
ΔV_0 (Å^3/SiO_2)	13.99	15.37	15.12	15.23	15.46	15.47	15.41	14.96	15.50	15.16	15.06	14.43[c]
P_t (GPa)	-0.37	6.94	2.71	3.79	3.84	2.66	2.48	6.16	6.55	3.99	6.24	7.46[a]
		7.2,[a] 6.2[b]										

[a]Reference 41.
[b]Reference 66.
[c]Reference 76.
[d]Reference 72.
[e]Reference 77.
[f]Reference 78.

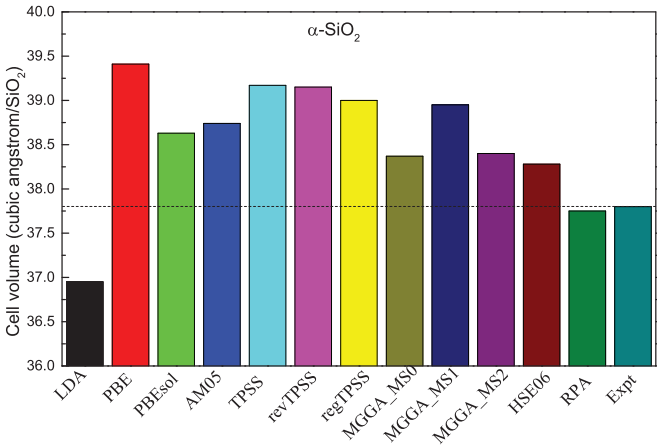

FIG. 4. (Color online) The equilibrium volumes of α-quartz calculated by different density functionals on Jacob's ladder. The results are compared with the experimental value. The dashed horizontal line is given to guide the eye.

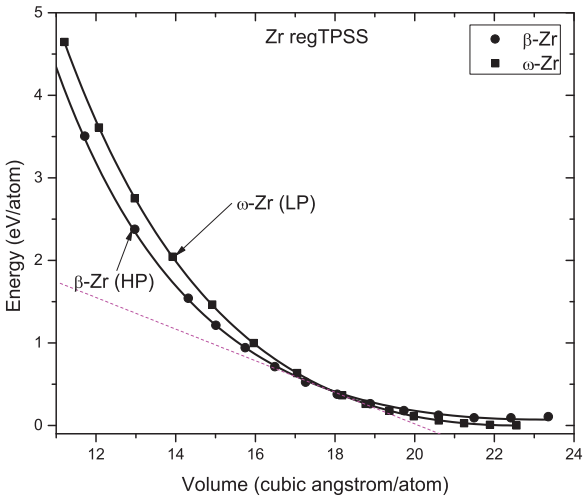

FIG. 5. (Color online) The volume dependencies of the total energies of the ω-Zr (LP) and β-Zr (HP) phases calculated using regTPSS. The solid lines are obtained by fitting the energy-volume data to the third-order Birch-Murnaghan equation of state, and the dashed line is the common tangent of the two energy-volume curves.

The calculated energy difference between α-quartz and stishovite is also given in Table II. LDA fails to predict that α-quartz is the ground state of SiO_2, so its ΔE_0 is negative (-0.031 eV/SiO_2). In experiment, this energy difference is found to be 0.51–0.54 eV per SiO_2, and the corresponding transition pressure from α-quartz to stishovite is 7.46 GPa.[41] Our PBE results are in good agreement with experiment and with previous PBE calculations. However, as for Si, the meta-GGAs other than those of the MGGA_MS family predict transition energies and pressures that are far too low. The phase transition parameters calculated from RPA ($\Delta E_0 = 0.39$ eV/SiO_2 and $P_t = 5.6$ GPa)[42] are less accurate than those from PBE, MGGA_MS0, and MGGA_MS1. As discussed in Ref. 42, RPA is less accurate for more molecular solids such as SiO_2 than it is for Si or metals. Note that the increase of transition pressure in SiO_2 system after including the thermal corrections is mainly due the entropy effects.[75]

C. ω-Zr-to-β-Zr phase transition

Both ω-Zr and β-Zr are normal metals, so their electron density distributions should be more uniform than those of the SiO_2 and Si systems. Since the approximate exchange-correlation functionals are usually constructed to be exact for the uniform electron gas, we would expect that the semilocal functionals can give better results for Zr than for the previous cases. As we shall see, that tends to be true, although the LDA and HSE06 transition pressures are rather unrealistic. A contravening effect is that the changes of energy and volume at the transition are much smaller in Zr than in the previous cases, so an accurate transition pressure requires them to have very small absolute errors.

Figure 5 shows the dependencies of the total energies of the two Zr phases on cell volume per atom using the regTPSS functional. The results for the other meta-GGA functionals are not shown for clarity, because the computed equilibrium cell volumes and energies of the ω-Zr and β-Zr structures are too close to the transition pressure. The common tangent line is also given in Fig. 5 for the two Zr phases.

In Table III, we show the structural properties and phase transition parameters for the two structures of Zr using different exchange-correlation functionals. The results are also compared to experiments. The most reliable transition pressure from ω-Zr to β-Zr was measured by Xia *et al.*[64] using the energy-dispersive x-ray diffraction method with a synchrotron light source, and the resulting value is 30 ± 2 GPa. In the same paper, for ω-Zr, the c/a ratio, bulk modulus, and pressure derivative of bulk modulus were also reported. However, the lattice constants and mechanical modulus of β-Zr were not accurately determined due to the limited pressure range applied in that experiment. The calculated lattice constants shown in Table III for the two Zr phases are compared with the experimental results reported by Hao *et al.*[62] and Greeff *et al.*[79]

All tested functionals yield accurate lattice constants for the Zr phases, with HSE06 the most accurate. The change of the equilibrium cell volume due to thermal expansion may be estimated from the zero-point anharmonic expansion for cubic crystals.[80] The Debye temperature (Θ_D) in this method can be calculated using Eq. (5) in Ref. 61. For the β-Zr phase, we use $\Theta_D = 269$ K computed using PW91 in a previous paper.[82] We applied the zero-point anharmonic expansion to correct the PBE cell volume. It was found that cell volume is slightly increased, i.e., 0.066 Å^3/atom, indicating that we can safely use lattice constants obtained at 0 K to draw our conclusion.

The bulk modulus of the ω-Zr phase predicted by different exchange-correlation functionals falls in the experimental range. The LDA lattice constants of β-Zr are too small, which results in the largest bulk modulus for this phase. The AM05 functional gives a rather small bulk modulus for the β-Zr phase, because this functional fails to show a reasonable minimum in the calculated energy-volume curve. The bulk moduli of the ω-Zr and β-Zr phases computed from HSE06 are smaller than from the semilocal functionals.

Tables II and III suggest that most semilocal functionals overestimate ΔV_0 somewhat in comparison with experiment. PBE and MGGA_MS2 work better than other tested

TABLE III. The structural properties and phase transition parameters of the ω-Zr (LP) and β-Zr (HP) phases. See Tables I and II for the definitions of ΔE_0 and ΔV_0. The ZPE and finite-temperature correction for the transition pressure have been evaluated from Debye's quasiharmonic approximation.[61] LDA and PBE give slightly different corrections for transition pressure due to ZPE and finite-T effect. For example, at 300 K, PBE gives -4 GPa and LDA gives -6 GPa. Our results in this paper were corrected by the PBE value reported in Ref. 61 for all functionals other than LDA, and by the LDA correction for the LDA functional.

Properties	LDA	PBE	PBEsol	AM05	TPSS	revTPSS	regTPSS	MGGA_MS0	MGGA_MS1	MGGA_MS2	HSE06	Expt.
						ω-Zr (hcp)						
a (Å)	4.9222	5.0235 5.056[a]	4.9715	4.9706	5.0045	4.9957	4.9892	5.0030	5.0090	5.0080	5.0240	5.039[a] 5.050[d]
c_0/a_0	0.6257	0.6246 0.6230[a]	0.6255	0.6255	0.6248	0.6248	0.6250	0.6269	0.6267	0.6244	0.6270	0.6251[a] 0.6237[d]
V_0 (Å^3/atom)	21.54	22.86	22.18	22.19	22.61	22.49	22.40	22.66	22.74	22.57	22.96	23.09[a]
B (GPa)	103.84	95.90 101.1,[a] 95.3[c]	100.2 4	99.0	99.04	99.73	99.39	95.52	97.24	100.24	91.05	104[b] 90,[e] 109[e]
B'	3.49	3.43 3.27,[a] 3.44[c]	3.45	3.43	3.44	3.41	3.41	3.42	3.37	3.34	3.34	2.05,[b] 4.0[e]
V_t (Å^3/atom)	17.68	18.60	18.04	18.03	18.46	18.31	18.29	18.50	18.53	18.47		
						β-Zr (bcc)						
a (Å)	3.4681	3.56 3.58[a]	3.5032	3.5173	3.5440	3.5347	3.5327	3.5414	3.5484	3.5440	3.5774	3.574[a] 3.570[c]
V_0 (Å^3/atom)	20.86	22.56	21.49	21.76	22.26	22.08	22.05	22.21	22.34	22.26	22.89	22.82[a]
B (GPa)	92.48	81.95 89.7[c]	87.52	76.51	86.08	83.95	86.40	82.14	82.17	84.93	78.59	
B'	3.71	3.60 3.13[c]	3.63	3.87	3.60	3.63	3.57	3.59	3.56	3.51	3.52	
V_t (Å^3/atom)	17.02	17.99	17.39	17.28	17.83	17.66	17.56	17.72	17.86	17.84		
						Phase transition parameters						
ΔE_0 (eV/atom)	0.059	0.084	0.075	0.078	0.087	0.087	0.088	0.113	0.109	0.123	0.200	
ΔV_0 (Å^3/atom)	0.690	0.300	0.685	0.432	0.352	0.410	0.362	0.450	0.400	0.320	0.065	0.270[a]
P_t (GPa)	9.17 5–24[h]	23.21 26.8,[a] 28.2,[f] 27,[g] 22[h]	17.06	23.28	22.56	21.78	26.62	31.25	27.01	28.08		30 $\pm$ 2[b]

[a]Reference 62.
[b]Reference 64.
[c]Reference 81.
[d]Reference 79.
[e]Reference 83.
[f]Reference 84.
[g]Reference 85.
[h]Reference 63.

TABLE IV. The equilibrium cell volumes of the Si, SiO_2, and Zr structures computed by DFT + D2 and optB86b-vdW methods, which introduce long-range van der Waals attraction. For the SiO_2 system, the unit is $Å^3/SiO_2$; for the other two systems it is $Å^3$/atom. The experimental values are not corrected for thermal effects, and the RPA value is used instead of the experimental value for β-tin Si to calculate the mean absolute error (MAE) of each functional. LP and HP indicate the low-pressure and high-pressure structures.

Structures	PBE + D2	TPSS + D2	optB86b-vdW	MGGA_MS0	RPA[a]	Expt.
D-Si (LP)	19.81	19.44	19.98	20.13	20.02	20.00[b]
β-tin Si (HP)	15.03	14.46	15.21	15.09	15.24	
α-quartz (LP)	38.75	37.02	34.56	38.37	37.75	37.73[c]
Stishovite (HP)	23.83	23.49	23.29	23.42	23.66	23.30[c]
ω-Zr (LP)	23.17	22.90	21.46	22.66		23.09[d]
β-Zr (HP)	22.53	22.19	21.13	22.21		22.82[d]
MAE	0.38	0.51	1.09	0.35		

[a]Reference 42.
[b]Reference 43.
[c]Reference 76.
[d]Reference 62.

exchange-correlation functionals for this parameter. The computed ΔV_0 for Zr from HSE06 is almost one order of magnitude smaller than those from other semilocal functionals. The main reason is that HSE06 underestimates the cell volume for ω-Zr, but slightly overestimates it for β-Zr, so that the errors reinforce each other instead of canceling.

For the phase transition parameter ΔE_0, PBE, TPSS, revTPSS, and regTPSS values are close to each other. The MGGA_MS values are slightly bigger. HSE06 seems to overestimate the energy difference between ω-Zr and β-Zr.

In contrast to Si and SiO_2 systems, the phonon corrections significantly affect the transition pressure from ω-Zr to β-Zr phases.[61] Hereafter, we only discuss the corrected results for different density functionals. As shown in Table III, PBE gives 23.2 GPa, which is slightly smaller than the experimental transition range. Without phonon corrections, our PBE value is in good agreement with Ref. 64. Using the same functional, Ostanin *et al.*[61] report 27.0 GPa at 300 K. The LDA overestimates the stability of the β-Zr phase, and the transition pressure is too small. In Ref. 61, the transition pressure calculated by LDA at 300 K is 18.0 GPa, which is larger than our LDA result (9.17 GPa). Cazorla *et al.*[63] obtained a value of 22 GPa from the WC functional, smaller than from PBE. Using a very rough relationship $P_t = \Delta E_0/\Delta V_0$ to estimate ω-Zr to β-Zr transition pressure, we find that the transition pressure is strongly overestimated by HSE06 (over 200 GPa). MGGA_MS0 yields 35.3 GPa without phonon effects (ZPE and finite $T = 300$ K). The transition pressure from ω-Zr to β-Zr phases is reduced to 31.3 GPa (very close to experiment) by including the two phonon corrections.

D. The effects of vdW interactions

The long-range vdW attraction is missing in LSDA, GGA, meta-GGA, and hybrid functionals. Sometimes it can be estimated by the pairwise-interaction DFT + D2 method of Grimme[70] or by the nonlocal density functional optB86b-vdW[86] method, both available in the VASP code. Table IV shows the equilibrium volumes predicted by these methods for our six phases. By comparison with Tables I–III, we see that the long-range corrections tend to decrease the cell volumes. OptB86b-vdW gives better cell volumes for stishovite, D-Si, and β-tin Si than DFT + D2 does. For α-quartz, the cell volume predicted by optB86b-vdW is too small, and RPA gives the best value. The nonempirical MGGA_MS0 functionals, which include some intermediate-range dispersion effects, give the best overall performance for equilibrium cell volume among all the tested methods.

The calculated phase transition pressures are illustrated in Fig. 6. For all three considered systems, the DFT + D2 methods are less accurate for phase transition pressure than their DFT counterparts. The TPSS + D2 method even predicts a negative transition pressure in the SiO_2 system. The optB86b-vdW works better for Si and Zr systems than for SiO_2. In the latter case, the transition pressure obtained from optB86b-vdW is smaller and less realistic than that from PBE and TPSS. In all three systems, MGGA_MS0 gives the best performance. Therefore, our calculations indicate that, for solids that are

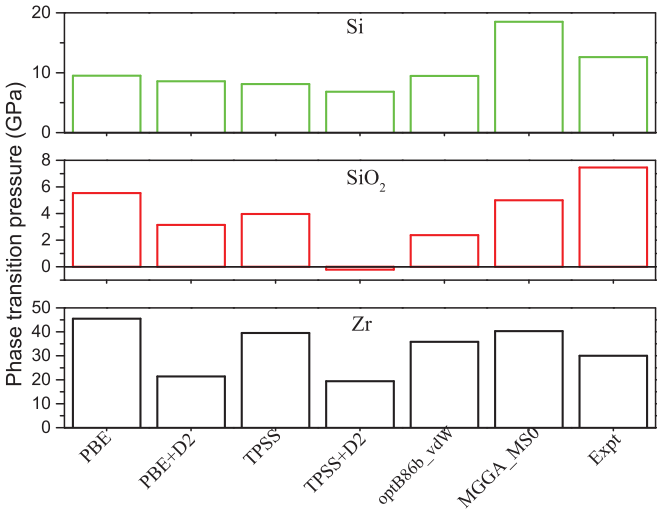

FIG. 6. (Color online) The computed phase transition pressures (P_t) for the Si, SiO_2, and Zr systems using DFT + D2 and optB86b-vdW methods to include long-range van der Waals corrections. Note that the values are estimated by $P_t = \Delta E_0/\Delta V_0$ for all methods, and thus are slightly different from those given in Tables I–III.

TABLE V. The electronic band gaps of the D-Si, α-quartz, and stishovite structures estimated from the calculated band-structure densities of states by semilocal and nonlocal functionals. The results of PW91 and WC were obtained using the CASTEP code. Our band gaps of the Si and SiO_2 systems were estimated from the calculated band dispersions using optimized crystal structures. Notice that the band gap of Si is indirect [$\Gamma = (0, 0, 0)$ to $X = (2\pi/a)\,(1, 1, 0)$]; α-quartz also has an indirect band gap [$K = (2\pi/a)\,(1/\sqrt{3}, 1/3, 0)$ to Γ]; the band gap of stishovite is direct at the Γ point. The unit of the band gap is eV.

Structure	LDA	PBE	PW91	PBEsol	AM05	WC	RPBE	TPSS	revTPSS	regTPSS	MGGA_MS0	MGGA_MS1	MGGA_MS2	HSE06	GW0	Expt
D-Si	0.49	0.62	0.73	0.49	0.52	0.57	0.70	0.38	0.25	0.25	0.17	0.22	0.22	1.14	1.22[a]	1.17[b]
α-quartz	5.68	5.70	6.06	5.70	5.84	5.94	5.70	5.94	5.50	5.52	5.60	5.55	5.59	7.50	9.40[c]	8.90[d]
Stishovite	5.90	5.13	5.77	5.47	5.42	5.68	4.95	5.56	5.17	5.17	4.25	4.28	4.38	8.06	8.90[a]	$5 \sim 6$[e] 8.75[f]

[a]Reference 87.
[b]Reference 88.
[c]Reference 89.
[d]Reference 90.
[e]Reference 91.
[f]Reference 92.

not primarily van der Waals bound, one should be cautious about using long-range vdW corrections for phase transition parameters and equilibrium lattice geometry.

IV. DISCUSSION

A. Structural vs transition properties

The meta-GGAs are generally good for structural properties. Except in α-quartz, all tested meta-GGAs perform as well as or better than even the PBEsol and AM05 GGAs for the equilibrium lattice constants and bulk moduli. Their overall performance for these two properties is much better than that of the LDA and PBE functionals.

From the results shown in Tables I–III in the previous section, we find that the calculated phase transition parameters are strongly dependent on the exchange-correlation functional employed, and even on the choice of meta-GGA, for all three solids, with the MGGA_MS meta-GGAs giving typically the best results. This intriguing conclusion may always be true as long as the energy and volume differences between the high- and low-pressure phases are small. The simplest explanation is suggested by the estimate $P_t = \Delta E_0/\Delta V_0$: A small change in either energy difference (ΔE_0) or volume difference (ΔV_0) affects the transition pressure significantly when the two quantities are very small.

The different behaviors of the screened hybrid functional HSE06 for insulating and metallic structures have been well documented and explained in previous works by Scuseria and co-workers.[93–95] They found that HSE functional has the right screening for semiconductors, but too much for large band gap insulators and not enough for metals.

B. Effect of the band gap

The calculated fundamental band gaps for D-Si, α-quartz, and stishovite by LDA, GGAs, meta-GGAs, HSE06, and GW_0 are given in Table V. Clearly, the most accurate band gaps are found by the HSE06 and GW_0 methods, in comparison with experimental values. Similar to LDA and GGAs, all tested meta-GGA functionals underestimate the band gaps for these three solids.

The underestimation of the fundamental band gap does not necessarily result in poor phase transition parameters for Si and SiO_2 systems, contrary to the suggestion of Ref. 43. The exact Kohn-Sham method should yield the exact transition parameters, but the band structure from even the exact Kohn-Sham multiplicative potential would underestimate the gap.[96,97]

In our calculations, only LDA and GGA have a multiplicative Kohn-Sham exchange-correlation potential $\delta E_{\rm xc}/\delta n(\vec{r})$, and they do indeed underestimate the gap. For computational convenience, our meta-GGA results employ a nonmultiplicative exchange-correlation potential which tends to underestimate the gap even more, and even when the transition parameters are good. The screened hybrid functional HSE06 includes a fraction of the nonmultiplicative Hartree-Fock exact exchange potential which increases and improves the single-particle band gap, in the same general way that the nonmultiplicative GW_0 self-energy does. With some effort, one could construct a multiplicative exchange-correlation

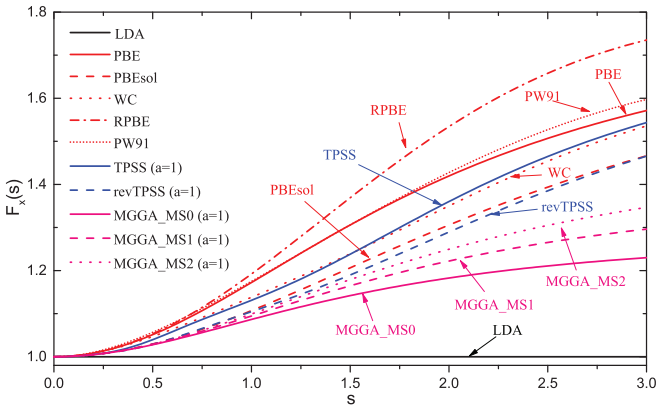

FIG. 7. (Color online) The exchange enhancement factors for various semilocal functionals. For meta-GGAs, $\alpha = 1$ and $s = 0$ correspond to uniform electron density.

potential for the meta-GGAs or hybrid functionals, which might yield GGA-like gaps without greatly changing the predicted transition parameters for these functionals.

C. Effect of the exchange enhancement factor

In some cases, we can relate a functional's performance for the transition parameters to the behavior of its plottable exchange enhancement factor F_x. Exchange is of course more important than correlation in the higher-density regions that contribute more to the total energy. Bonding regions also tend to have small s.

First consider the LDA and GGA functionals. Figure 7 shows $F_x(s)$ in the physically important range $0 < s < 3$. $F_x(s)$ equals 1 in LDA at all s and in GGA at $s = 0$. Within GGA, it increases with s, and the initial strength of this increase grows from LDA to PBEsol to PBE to RPBE. Tables I–III suggest that the predicted transition pressures tend to increase in the same order.

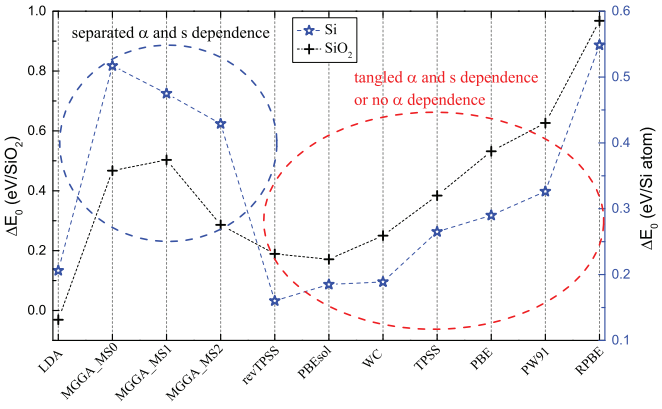

FIG. 8. (Color online) The calculated structural energy differences of Si (right vertical scale) and SiO_2 (left vertical scale) polymorphs from semilocal functionals on the first three rungs of Jacob's ladder. The results imply that an α dependence of F_x separated from the s dependence can significantly improve the energy difference between two polymorphs of a solid.

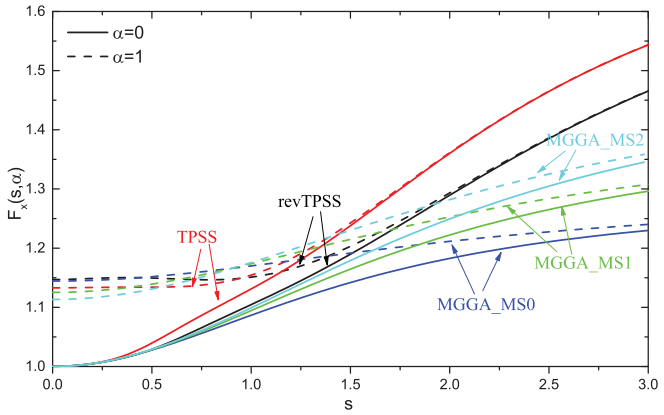

FIG. 9. (Color online) The exchange enhancement factors of meta-GGA functionals for the $\alpha = 0$ and $\alpha = 1$ limits.

For the phase transition parameters, systematic improvement over GGAs and LDA is not seen for most meta-GGAs, but only for the MGGA_MS variants. The main difference between the MGGA_MS family of density functionals and other tested functionals lies in the exchange enhancement factor $F_x(s,\alpha)$, where the weaker s dependence in MGGA_MS (Fig. 7) is countered by a stronger α dependence. Our recent work has revealed the significance of α for identifying different bonds in molecules and solids.[30,98] The covalent-single and metallic bonds are characterized by $\alpha = 0$ and 1, respectively. Weak bonds such as van der Waals are characterized by $\alpha \gg 1$. By carefully manipulating both α and s dependencies in a meta-GGA exchange functional, one can describe all different types of chemical bonds more accurately than with the ordinary GGAs and LDA. The influences of α and s on the calculated phase transition parameters for Si and SiO_2 systems are illustrated in Fig. 8.

Figure 9 shows the enhancement factors of various meta-GGAs at $\alpha = 0$ and 1. The small-s behavior is like that of GGA ($F_x \approx 1$) only for $\alpha = 1$, with $F_x \approx 1.15$ at $\alpha = 0$.

Figures 10 and 11 show in detail how $F_x(s,\alpha)$ varies over the s-α plane, first for revTPSS (which yields unrealistically low transition pressures for Si and SiO_2), and then for MGGA_MS (which is much more realistic). The α dependence at $s \approx 0$ reveals two qualitative differences between these two meta-GGAs: (1) The MGGA_MS F_x drops gradually from $\sim$1.15 to $\sim$1 as α increases from 0 to 1, while the revTPSS F_x drops abruptly near $\alpha = 0$ and then remains close to 1. (2) The MGGA_MS continues to drop well below 1 as α increases above 1, while the revTPSS does not. Feature (2) is responsible for the much better description of the intermediate-range van der Waals interaction by MGGA_MS.

Figures 12 and 13 plot $r_s = (3/[4\pi n])^{1/3}$, s and α along a line through a bond in the low-pressure phases of Si and SiO_2. The line for each solid is defined in the Supplemental Material,[99] which also provides more detailed contour plots. Figures 12 and 13 also show the meta-GGA exchange energy density $n\varepsilon_x^{\text{unif}} F_x$ (which need not be in the same gauge as the conventional exact exchange energy density). Note that we use pseudoatoms instead of real ones, and that the pseudodensity is low (i.e., r_s is large) in the core regions.

First consider the phase transition in Si. The high-pressure phase β-tin is metallic, with $s \ll 1$ and $\alpha \approx 1$ in the bonding

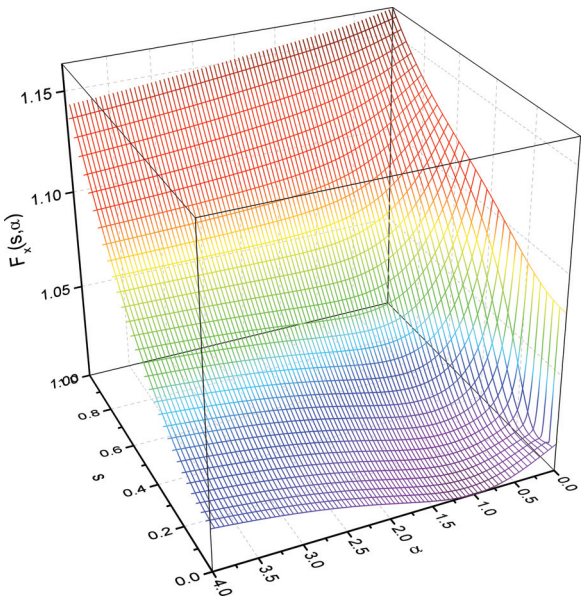

FIG. 10. (Color online) The exchange gradient enhancement factor $F_x(s,\alpha)$ of revTPSS as a function of s and α, showing the order-of-limits problem when $s \approx 0$ and $\alpha \approx 0$. Note that when $s = 0$ and α goes to infinity, $F_x\ (s,\alpha) \approx 1.035$.

regions, so all tested functionals have similar exchange energy density there. But the low-pressure phase D-Si gets a much more negative exchange energy density in the bonding regions from MGGA_MS than from PBE or revTPSS, as shown in Fig. 12. This arises because of feature (1) above, since the covalent single-bonding regions of D-Si have both small s and small α. Thus MGGA_MS energetically stabilizes D-Si with respect to β-tin, increasing the transition energy difference and the transition pressure.

Next consider the transition in SiO_2, where there is strong electron transfer from Si to O in each phase. Reference 100 indicates that the Si-O bonds in stishovite even show a stronger ionic character than those of α-quartz. As a result,

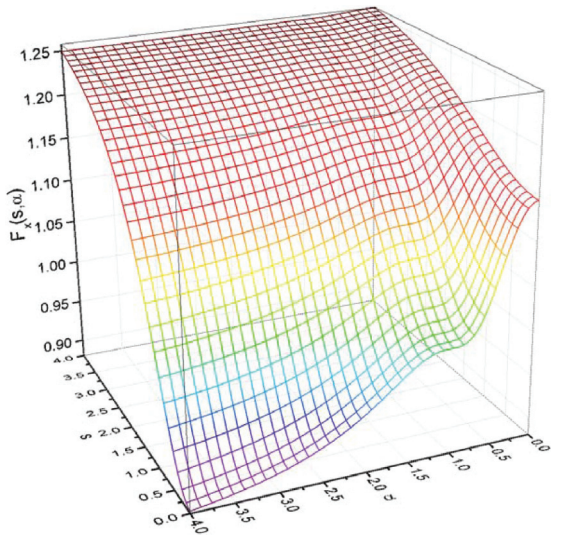

FIG. 11. (Color online) The same as Fig. 10, but for MGGA_MS0. Note that the scales for s are different in Figs. 10 and 11.

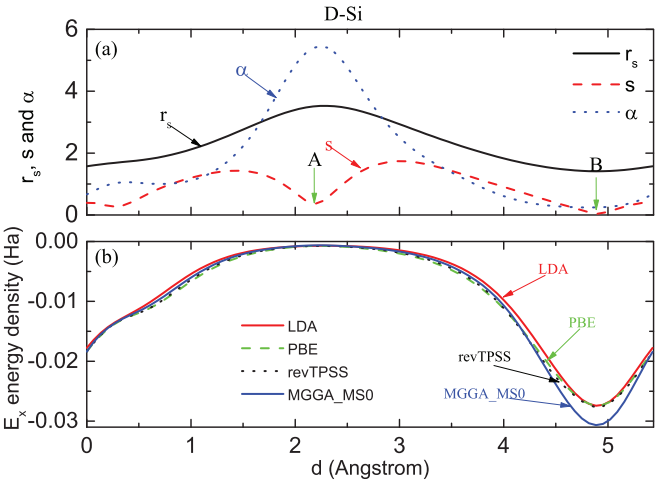

FIG. 12. (Color online) (a) The computed r_s, s, and α distributions along a line in the [001] direction, within the (110) plane and passing through the bond center, for the D-Si (LP) crystal using the LDA density. (b) The exchange energy densities along the same path by LDA, GGAs, and meta-GGAs. A and B indicate the interstitial and single bond regions, respectively.

in stishovite, we have O^{2-} ions weakly overlapped with Si^{4+} ions. The overlap of the two ten-electron closed shells leads to large α in the bond region, just as we would have for two overlapped Ne atoms. But in this case the resulting van der Waals interactions are totally overwhelmed by the electrostatic attraction. Therefore, the tested functionals yield similar exchange energy densities for the low-pressure phase α-quartz, as shown in Fig. 13. But the high-pressure phase stishovite has large values of α in the bonding region (Fig. SIII of the Supplemental Material[99]); so feature (2) above yields a much less negative exchange energy density from MGGA_MS than from PBE or revTPSS. This MGGA_MS energetically destabilizes stishovite with respect to α-quartz, again increasing the transition energy difference and the transition pressure.

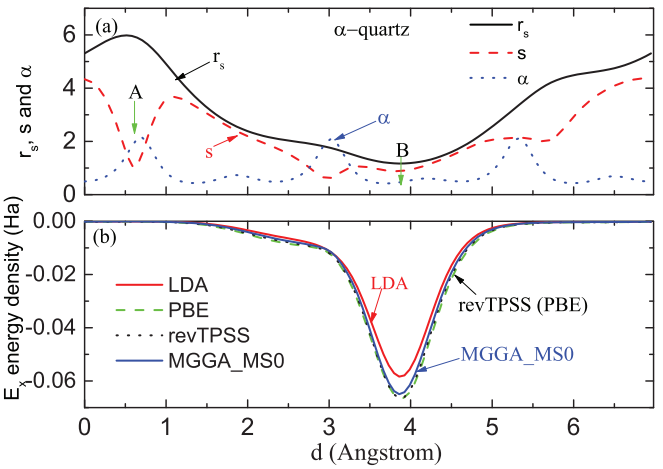

FIG. 13. (Color online) The same as Fig. 12, but for α-quartz SiO_2 (LP). A and B label the interstitial and Si-O bond regions along a line in the [001] direction on the (100) plane.

V. CONCLUSIONS

We have tested the performance of LSDA, the PBE GGA, and several meta-GGA functionals (TPSS, revTPSS, regTPSS, and MGGA_MS) on the structural properties and phase transition parameters for three different systems, i.e., Si, SiO_2, and Zr. For the structural properties, all tested meta-GGAs are better than the PBE GGA, as expected, but for the phase transition pressures the earlier meta-GGAs are worse than PBE for Si and SiO_2, and only the members of the MGGA_MS family are able to predict realistic values. The quality of the results is sensitive to the details of the exchange functional. At least for the insulator-to-metal transition in Si, the relative performance of various functionals can be understood simply in terms of their plottable exchange enhancement factors. We suggest that further improvements to the meta-GGA will lead to further improvements in the predicted properties of most molecules and solids near equilibrium and under pressure, without sacrificing computational efficiency.

Our results for normal metals (Zr phases) indicate that all semilocal functionals perform more or less similarly for equilibrium lattice constants and bulk modulus. Some meta-GGA functionals (regTPSS and MGGA_MS) can predict phase transition parameters for Zr in better agreement with experiment than PBE. For this system, the screened hybrid functional HSE06 significantly overestimates phase transition parameters (transition energy and pressure). Although the tested functionals are all more accurate for the metallic Zr phases than for Si or SiO_2, the exceptionally small structural energy and volume differences for Zr still make this system challenging to approximate calculations.

For the transition pressure in general, the approximate exchange-correlation energy functional must predict a small energy difference with a small relative error. That is not so hard when the small energy difference arises from a small change in the electron density, because then we can expect a great error cancellation in the energy difference between similar densities. That explains how even LSDA can predict rather good lattice constants in some cases: There is a small change of density associated with a small expansion or compression of the lattice. But, for the transition pressure, we have to predict a small energy difference arising from a large change of density, and less error cancellation can be expected. Therefore, the calculation of transition pressures for structural phase transitions remains a challenging test of density functionals. The challenge is especially great for silicon dioxide, where the average valence electron density changes so strongly at the transition.

ACKNOWLEDGMENTS

This work was supported by the National Science Foundation under Grants No. DMR-0854769 and No. DMR-1305135 (J.P.P.) and by the Department of Energy under Grant No. DE-SC0010499 (A.R.). Most calculations were carried out using clusters provided by the Louisiana Optical Network Initiative (LONI: http://www.loni.org/) and also by the Center for Computational Science at Tulane University. R.H. thanks the Deutsche Forschungsgemeinschaft (DFG Grant No. HA 5711/2-1). The work at Rice University was supported by the National Science Foundation under Grant No. CHE-1110884 and the Welch Foundation (C-0036).

*tuf23889@temple.edu

[1] P. Hohenberg and W. Kohn, Phys. Rev. **136**, B864 (1964).
[2] W. Kohn and L. J. Sham, Phys. Rev. **140**, A1133 (1965).
[3] W. Kohn, Rev. Mod. Phys. **71**, 1253 (1999).
[4] J. P. Perdew and S. Kurth, in *A Primer for Density Functional Theory*, edited by C. Fiolhais, F. Nogueira, and M. Marques, Lecture Notes in Physics Vol. 620 (Springer, Berlin, 2003), Chap. 1.
[5] J. P. Perdew and A. Ruzsinszky, Rev. Mineral. Geochem. **71**, 1 (2010).
[6] J. P. Perdew, A. Ruzsinszky, J. Tao, V. N. Staroverov, G. E. Scuseria, and G. I. Csonka, J. Chem. Phys. **123**, 062201 (2005).
[7] J. P. Perdew and K. Schmidt, in *Density Functional Theory and Its Application to Materials*, edited by V. Van Doren, C. Van Alsenoy, and P. Geerlings, AIP Conf. Proc. No. 577 (AIP, Melville, NY, 2001).
[8] A. Ruzsinszky, J. P. Perdew, and G. I. Csonka, J. Chem. Theory. Comput. **6**, 127 (2010).
[9] J. P. Perdew, K. Burke, and M. Ernzerhof, Phys. Rev. Lett. **77**, 3865 (1996).
[10] Y. Zhang and W. Yang, Phys. Rev. Lett. **80**, 890 (1998).
[11] B. Hammer, L. B. Hansen, and J. K. Norskov, Phys. Rev. B **59**, 7413 (1999).
[12] R. Armiento and A. E. Mattsson, Phys. Rev. B **72**, 085108 (2005).
[13] A. E. Mattsson and R. Armiento, Phys. Rev. B **79**, 155101 (2009).
[14] Z. Wu and R. E. Cohen, Phys. Rev. B **73**, 235116 (2006).
[15] J. P. Perdew, A. Ruzsinszky, G. I. Csonka, O. A. Vydrov, G. E. Scuseria, L. A. Constantin, X. L. Zhou, and K. Burke, Phys. Rev. Lett. **100**, 136406 (2008).
[16] Y. Zhao and D. G. Truhlar, J. Chem. Phys. **128**, 184109 (2008).
[17] J. P. Perdew, L. A. Constantin, E. Sagvolden, and K. Burke, Phys. Rev. Lett. **97**, 223002 (2006).
[18] J. Sun, M. Marsman, G. I. Csonka, A. Ruzsinszky, P. Hao, Y. S. Kim, G. Kresse, and J. P. Perdew, Phys. Rev. B **84**, 035117 (2011).
[19] J. P. Perdew, Phys. Rev. Lett. **55**, 1665 (1985).
[20] S. K. Ghosh and R. G. Parr, Phys. Rev. A **34**, 785 (1986).
[21] A. D. Becke and M. R. Roussel, Phys. Rev. A **39**, 3761 (1989).
[22] T. Van Voorhis and G. E. Scuseria, J. Chem. Phys. **109**, 400 (1998).
[23] H. L. Schmider and A. D. Becke, J. Chem. Phys. **109**, 8188 (1998).
[24] J. P. Perdew, S. Kurth, A. Zupan, and P. Blaha, Phys. Rev. Lett. **82**, 2544 (1999).
[25] J. Tao, J. P. Perdew, V. N. Staroverov, and G. E. Scuseria, Phys. Rev. Lett. **91**, 146401 (2003).
[26] J. P. Perdew, A. Ruzsinszky, G. I. Csonka, L. A. Constantin, and J. Sun, Phys. Rev. Lett. **103**, 026403 (2009).
[27] Y. Zhao and D. G. Truhlar, J. Chem. Phys. **125**, 194101 (2006).
[28] A. Ruzsinszky, J. Sun, B. Xiao, and G. I. Csonka, J. Chem. Theory. Comput. **8**, 2078 (2012).
[29] J. Sun, B. Xiao, and A. Ruzsinszky, J. Chem. Phys. **137**, 051101 (2012).

[30]J. Sun, R. Haunschild, B. Xiao, G. E. Scuseria, and J. P. Perdew, J. Chem. Phys. **138**, 044113 (2013).
[31]G. L. Oliver and J. P. Perdew, Phys. Rev. A **20**, 397 (1979).
[32]J. Sun, B. Xiao, Y. Fang, R. Haunschild, P. Hao, A. Ruzsinszky, G. I. Csonka, G. E. Scuseria, and J. P. Perdew, Phys. Rev. Lett. **111**, 106401 (2013).
[33]L. A. Curtis, K. Raghavachari, P. C. Redfern, and J. A. Pople, J. Chem. Phys. **106**, 1063 (1997).
[34]L. A. Curtis, P. C. Redfern, K. Raghavachari, and J. A. Pople, J. Chem. Phys. **109**, 42 (1998).
[35]Y. Zhao, B. J. Lynch, and D. G. Truhlar, J. Phys. Chem. A **108**, 2715 (2004).
[36]P. Haas, F. Tran, and P. Blaha, Phys. Rev. B **79**, 085104 (2009).
[37]V. N. Staroverov, G. E. Scuseria, J. Tao, and J. P. Perdew, Phys. Rev. B **69**, 075102 (2004).
[38]P. Hao, Y. Fang, J. Sun, G. I. Csonka, P. H. T. Philipsen, and J. P. Perdew, Phys. Rev. B **85**, 014111 (2012).
[39]L. Schimka, J. Harl, A. Stroppa, A. Gruneis, M. Marsman, F. Mittendorfer, and G. Kresse, Nat. Mater. **9**, 741 (2010).
[40]J. Sun, M. Marsman, A. Ruzsinszky, G. Kresse, and J. P. Perdew, Phys. Rev. B **83**, 121410(R) (2011).
[41]D. R. Hamann, Phys. Rev. Lett. **76**, 660 (1996).
[42]B. Xiao, J. Sun, A. Ruzsinszky, J. Feng, and J. P. Perdew, Phys. Rev. B **86**, 094109 (2012).
[43]R. G. Hennig, A. Wadehra, K. P. Driver, W. D. Parker, C. J. Umrigar, and J. W. Wilkins, Phys. Rev. B **82**, 014101 (2010).
[44]E. R. Batista, J. Heyd, R. G. Hennig, B. P. Uberuaga, R. L. Martin, G. E. Scuseria, C. J. Umrigar, and J. W. Wilkins, Phys. Rev. B **74**, 121102(R) (2006).
[45]G. Kresse and D. Joubert, Phys. Rev. B **59**, 1758 (1999).
[46]J. Harl, L. Schimka, and G. Kresse, Phys. Rev. B **81**, 115126 (2010).
[47]H. J. Monkhorst and J. D. Pack, Phys. Rev. B **13**, 5188 (1976).
[48]J. P. Perdew and A. Zunger, Phys. Rev. B **23**, 5048 (1981).
[49]J. E. Peralta, J. Heyd, G. E. Scuseria, and R. L. Martin, Phys. Rev. B **74**, 073101 (2006).
[50]F. Tran, P. Blaha, K. Schwarz, and P. Novak, Phys. Rev. B **74**, 155108 (2006).
[51]K. Hummer, J. Harl, and G. Kresse, Phys. Rev. B **80**, 115205 (2009).
[52]J. Wrobel, K. J. Kurzydlowski, K. Hummer, G. Kresse, and J. Piechota, Phys. Rev. B **80**, 155124 (2009).
[53]J. P. Perdew, J. A. Chevary, S. H. Vosko, K. A. Jackson, M. R. Pederson, D. J. Singh, and C. Fiolhais, Phys. Rev. B **46**, 6671 (1992).
[54]M. D. Segall, P. J. D. Lindan, M. J. Probert, C. J. Pickard, P. J. Hasnip, S. J. Clark, and M. C. Payne, J. Phys.: Condens. Matter. **14**, 2717 (2002).
[55]R. Maezono, N. D. Drummond, A. Ma, and R. J. Needs, Phys. Rev. B **82**, 184108 (2010).
[56]S. Gaurav, B. S. Sharma, S. B. Sharma, and S. C. Upadhyaya, Physica B **322**, 328 (2002).
[57]A. Otero-de-la-Roza and V. Luaña, Comput. Phys. Commun. **182**, 1708 (2011).
[58]R. J. Needs and R. M. Martin, Phys. Rev. B **30**, 1773 (1984).
[59]A. Werner, J. A. Sanjurjo, and M. Cardona, Solid State Commun. **44**, 155 (1982).
[60]P. Kroll, M. Milko, and Z. Anorg, Allg. Chem. **629**, 1737 (2003).
[61]S. A. Ostanin and V. Y. Trubitsin, Phys. Rev. B **57**, 13485 (1998).
[62]Y. J. Hao, L. Zhang, X. R. Chen, Y. H. Li, and H. L. He, J. Phys.: Condens. Matter. **20**, 235230 (2008).
[63]C. Cazorla, D. Alfe, and M. J. Gillan, Phys. Rev. B **77**, 224103 (2008).
[64]H. Xia, S. J. Duclos, A. L. Ruoff, and Y. K. Vohra, Phys. Rev. Lett. **64**, 204 (1990).
[65]J. Z. Hu, L. D. Merkle, C. S. Menoni, and I. L. Spain, Phys. Rev. B **34**, 4679 (1986).
[66]A. Zupan, P. Blaha, K. Schwarz, and J. P. Perdew, Phys. Rev. B **58**, 11266 (1998).
[67]K. Gaal-Nagy, A. Bauer, M. Schmitt, K. Karch, P. Pavone, and D. Strauch, Phys. Status Solidi B **211**, 275 (1999).
[68]K. J. Chang and M. L. Cohen, Phys. Rev. B **31**, 7819 (1985).
[69]J. Harl and G. Kresse, Phys. Rev. B **77**, 045136 (2008).
[70]S. Grimme, J. Comput. Chem. **27**, 1787 (2006).
[71]J. Paier, M. Marsman, K. Hummer, G. Kresse, I. C. Gerber, and J. G. Angyan, J. Chem. Phys. **124**, 154709 (2006).
[72]L. G. Liu, Mech. Mater. **14**, 283 (1993).
[73]J. S. Weaver, D. W. Chipman, and T. Takahashi, Am. Mineral. **64**, 604 (1979).
[74]K. P. Driver, R. E. Cohen, Z. Wu, B. Militzer, P. López Ríos, M. D. Towler, R. J. Needs, and J. W. Wilkins, Proc. Nat. Acad. Sci. USA **107**, 9519 (2010).
[75]C. Lee and X. Gonze, Phys. Rev. B **51**, 8610 (1995)
[76]B. B. Karki, M. C. Warren, L. Stixrude, G. J. Ackland, and J. Crain, Phys. Rev. B **55**, 3465 (1997).
[77]H. D'Amour, W. Denner, and H. Schulz, Acta. Crystallogr., Sect. B: Struct. Crystallogr. Cryst. Chem. B **35**, 550 (1979).
[78]J. C. Boettger, J. Appl. Phys. **72**, 5500 (1992).
[79]C. W. Greeff, Modell. Simul. Mater. Sci. Eng. **13**, 1015 (2005).
[80]G. I. Csonka, J. P. Perdew, A. Ruzsinszky, P. H. T. Philipsen, S. Lebègue, J. Paier, O. A. Vydrov, and J. G. Ángyán, Phys. Rev. B **79**, 155107 (2009).
[81]S. L. Shang, A. Saengdeejing, Z. G. Mei, D. E. Kim, H. Zhang, S. Ganeshan, Y. Wang, and Z. K. Liu, Comput. Mater. Sci. **48**, 813 (2010).
[82]Q. Chen and B. Sundman, Acta. Mater. **49**, 947 (2001).
[83]Y. Zhao, J. Zhang, C. Pantea, J. Qian, L. L. Daemen, P. A. Rigg, R. S. Hixson, G. T. Gray, Y. Yang, L. Wang, Y. Wang, and T. Uchida, Phys. Rev. B **71**, 184119 (2005).
[84]I. Schnell and R. C. Albers, J. Phys.: Condens. Matter **18**, 1483 (2006).
[85]K. D. Joshi, G. Jyoti, S. C. Gupta, and S. K. Sikka, J. Phys.: Condens. Matter **14**, 10921 (2002).
[86]J. Klimeš, D. R. Bowler, and A. Michaelides, Phys. Rev. B **83**, 195131 (2011).
[87]The GW_0 calculations were performed for D-Si and stishovite phases with their experimental lattice constants using the VASP code. The calculation parameters we applied are given below for stishovite: The kinetic energy cutoff (E_{cut}) was set to 400 eV, and the k mesh to $7 \times 7 \times 9$. The frequency dependence of the dielectric function was evaluated using 300 Kohn-Sham LDA orbitals. The convergence of the band gap has been carefully confirmed using smaller E_{cut} (380 eV) and k mesh ($6 \times 6 \times 8$), and also fewer Kohn-Sham orbitals (200). For the D-Si phase, we used 350 eV, $8 \times 8 \times 8$ and 96 for E_{cut}, k mesh, and the number of Kohn-Sham LDA orbitals, respectively. Within the present settings, the quasiparticle band gap was converged to 0.01 eV.

[88]L. Schimka, J. Harl, and G. Kresse, J. Chem. Phys. **134**, 024116 (2011).
[89]G. Kresse, M. Marsman, L. E. Hintzsche, and E. Flage-Larsen, Phys. Rev. B **85**, 045205 (2012).
[90]R. B. Laughlin, Phys. Rev. B **22**, 3021 (1980).
[91]G. Wiech, Solid State Commun. **52**, 807 (1984).
[92]A. N. Trukhin, T. I. Dyuzheva, L. M. Lityagina, and N. A. Bendeliani, Solid State Commun. **131**, 1 (2004).
[93]T. M. Henderson, J. Paier, and G. E. Scuseria, Phys. Status Solidi B **248**, 767 (2011).
[94]M. J. Lucero, T. M. Henderson, and G. E. Scuseria, J. Phys. Condens. Matter **24**, 145504 (2012).
[95]X.-D. Wen, R. L. Martin, T. M. Henderson, and G. E. Scuseria, Chem. Rev. **113**, 1063 (2013).
[96]J. P. Perdew, R. G. Parr, M. Levy, and J. L. Balduz, Phys. Rev. Lett. **49**, 1691 (1982).
[97]C. C. Wang, J. V. James, and J. F. Xia, Phys. Rev. Lett. **51**, 184 (1983).
[98]Y. Fang, B. Xiao, J. Tao, J. Sun, and J. P. Perdew, Phys. Rev. B **87**, 214101 (2013).
[99]See Supplemental Material at http://link.aps.org/supplemental/10.1103/PhysRevB.88.184103 for the two-dimensional (2-D) contour plots of Wigner-Seitz radius (r_s), reduced density gradient (s) and α distributions are illustrated for D-Si (110 plane) and α-quartz (100 plane). For stishovite, we only show the α distribution at ($\bar{1}10$) plane.
[100]D. Li, G. M. Bancroft, M. Kasrai, M. E. Fleet, R. A. Secco, X. H. Feng, K. H. Tan, and B. X. Yang, Am. Mineral. **79**, 622 (1994).